CHAPTER 6

GARCINIA CAMBOGIA EXTRACT: NATURAL CORROSION INHIBITOR FOR MILD STEEL IN ACID MEDIA

This chapter illustrates the corrosion-resistant power of the ethanol extract of *Garcinia cambogia* (GCE) leaves for mild steel in 1 M HCl and 0.5 M H_2SO_4. Gravimetric, electrochemical and morphological studies have been established to authenticate inhibiting power of GCE. Although GCE contains numerous bioactive components, organic acids such as hydroxycitric acid (HCA) and hydroxycitric acid lactone HCA lactone) (Fig. 6.1) are the leaf extract's primary class of compounds[173]. Quantum mechanical investigations of HCA and HCA lactone have been established the anticorrosion behaviour of GCE.

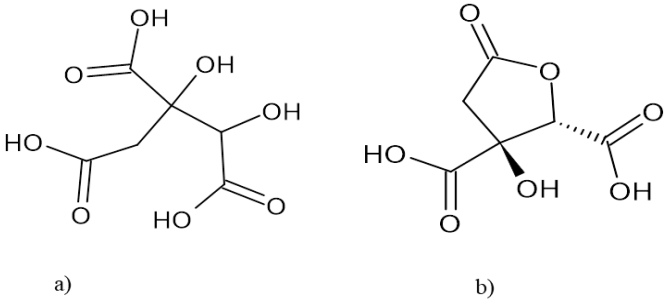

Fig. 6.1: Structure of a) hydroxycitric acid b) hydroxycitric acid lactone

Garcinia cambogia

Results and discussions

Phytochemical screening of GCE

Based on the standard screening tests, major phytochemicals in GCE were confirmed, and the results are given in Table 6.1.

FTIR spectroscopy

Fig. 6.2 shows the FTIR spectrum of GCE, which revealed characteristic stretching and bending frequencies for various bonds. Broad band at 3281 cm^{-1} indicates O-H stretching vibration, which is a hydrogen bonding band. Two sharp peaks at 2917

cm^{-1} and 2850 cm^{-1} exhibit alkyl C-H stretching bonds. >C=O stretching band occurs at 1731 cm^{-1}. This peak may be assigned to carboxylic acids. The peaks at 1622 cm^{-1} and 1463 cm^{-1} can be accredited to aliphatic and aromatic C=C stretching vibrations. C-O stretching vibration appears as a weak band at 1242 cm^{-1} and 1031 cm^{-1}. In short, well-defined peaks of GCE can be ascribed to heteroatoms, aromatic rings, and unsaturated compounds.

Table 6.1: Phytochemical screening of GCE

Sl. No.	Compounds	Tests	Results
1	Alkaloids	Mayers reagent	−−
2	Steroids	Salkowaski's test	++
3	Phenolic compounds	Potassium ferrocyanide test	++
4	Flavanoids	Sodium hydroxide test	++
5	Saponins	Froth test	++
6	Tannins	Lead acetate test	++
7	Cardiac glycosides	Conc. sulphuric acid test	++
8	Coumarin	Alcoholic NaOH test	−−
9	Quinones	Conc. sulphuric acid test	++

++ (present), − − (Absent)

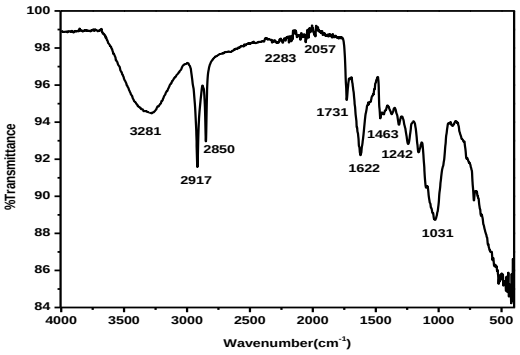

Fig. 6.2: FTIR spectrum of GCE

Weight loss measurements

❖ ***Effect of concentration***

The period of the adsorption layer's existence on the metal surface can be estimated in weight loss measurements. The inhibition efficiency (ɳ%) and corrosion rate (υ) were tabulated in Table 6.2. It can be seen that as GCE concentration raised, metal

corrosion potency also got increased in 1 M HCl and 0.5 M H_2SO_4 solutions. Weight loss measurement is a long-term measurement that may differ considerably from short-term methods like electrochemical techniques. Because the previous one corresponds to the steady-state of the corrosion process, whereas the latter results in instantaneous corrosion rates.

Table 6.2: Weight loss measurements of mild steel with and without GCE in 1 M HCl and 0.5 M H_2SO_4 at room temperature for 24 hrs

Conc. (v/v %)	Corrosion rate (mm/yr)		Inhibition efficiency (η%)	
	1 M HCl	0.5 M H_2SO_4	1 M HCl	0.5 M H_2SO_4
Blank	3.95	35.57	-	-
1	1.77	18.83	55.12	47.06
2	1.44	16.92	63.49	52.41
3	1.20	15.08	69.53	57.59
4	1.08	13.22	72.48	62.82
5	0.32	8.70	91.73	75.53

GCE exhibited a lower η% value of 55.12% at a minimum concentration (1 v/v%) and an extreme η% value of 91.73% at the highest concentration (5 v/v%) in 1 M HCl at room temperature. In hydrochloric acid medium, GCE exhibited reasonably better metal corrosion inhibition efficacy than in sulphuric acid medium. In 0.5 M H_2SO_4, maximum η% reached 75.53% at 5 v/v%. Surface coverage is the determining factor for corrosion inhibition potential. At higher GCE concentrations, the number of obtainable inhibitor molecules built on the metal surface led to higher surface coverage and reduced acidic corrosion for mild steel. The electron-donating ability of hydroxyl groups, heteroatoms and unsaturated compounds present in GCE can be accredited to the inhibition capacity of GCE, which is comprised of multi-complex compounds. HCA has also sustained high electron density towards the metal surface. The extent of hydration of chloride ions is smaller than sulphate ions. It may cause specific adsorption of

chloride ions compared to sulphate ions[174]. Since the number of adsorbed Cl^- ions on the metal surface is sufficient to generate negative charges towards the acid media, the cationic form of hydroxycitric acid adsorbs to a large extent.

❖ ***Effect of temperature***

The influence of temperature on the metal dissolution process was analyzed by employing weight loss measurements at four different temperatures 303, 313, 323 and 333 K. Variation in corrosion rate and inhibition efficiency is depicted in Fig. 6.3 and is computed in Table 6.3.

It is evident from the data that temperature is directly proportional to the rate of corrosion. When the temperature increased from 303 K to 333 K, inhibition potency showed a noticeable decrease from 91.73% to 72.08% for 5% GCE concentration in HCl solution. Likewise, in the H_2SO_4 medium, inhibition potency decreased from 75.53% to 62.46% for the highest concentration under study. This trend may be attributed to the desorption of GCE molecules from the metal surface at elevated temperatures and thereby destroys protection film and causes metal destruction.

Arrhenius equation (41) was applied to calculate the activation energy of metal corrosion. Fig. 6.4 a) and Fig. 6.5 a) represent the plot of log K vs 1/T for mild steel in acid media with and without GCE. The equation (43) derived from transition state theory was employed to acquire thermodynamic parameters such as enthalpy of activation (ΔH^*) and entropy of activation (ΔS^*) values. Slope and intercept of the plot of log K/T vs 1/T (Fig. 6.4 b) and Fig. 6.5 b)) corresponds to ΔH^* and ΔS^* values. All the thermodynamic parameters were calculated in Table 6.4, involving activation energy (E_a) and pre-exponential factor (A). Examining Table 6.4, it was clear that the acid solution without GCE has more activation energy of metal corrosion than the acid solution with GCE. The increase in E_a values with GCE concentration causes a reduction in the metal

dissolution rate[175]. Endothermic behaviour of metal corrosion was revealed from the positive values of the enthalpy of activation. As the concentration of GCE increased, ΔH* and ΔS* values were also raised.

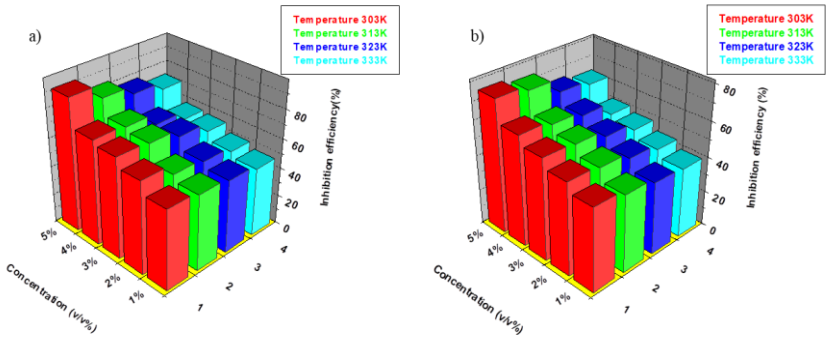

Fig. 6.3: Variation in inhibition efficiency of GCE in a) 1 M HCl b) 0.5 M H_2SO_4 at elevated temperatures

Table 6.3: Corrosion rate (υ) and inhibition efficiency (η%) of GCE in 1 M HCl and 0.5 M H_2SO_4 at different temperatures for 24 hrs

Medium	Conc. (v/v%)	υ (303 K)	η% (303 K)	υ (313 K)	η% (313 K)	υ (323 K)	η% (323 K)	υ (333 K)	η% (333 K)
1 M HCl	Blank	3.95	-	13.11		22.05	-	31.77	-
	1	1.77	55.12	6.23	52.48	10.94	50.40	16.78	47.18
	2	1.44	63.49	5.72	56.37	10.09	54.25	15.56	51.02
	3	1.20	69.53	4.15	68.34	8.13	63.14	13.69	56.91
	4	1.08	72.48	3.79	71.09	8.05	63.50	13.28	58.20
	5	0.32	91.73	2.26	82.76	5.01	77.28	8.87	72.08
0.5 M H_2SO_4	Blank	35.57	-	58.27	-	86.25	-	106.2	-
	1	18.83	47.06	32.69	43.89	50.95	40.92	64.14	39.63
	2	16.92	52.41	28.58	50.95	45.58	47.15	59.64	43.87
	3	15.08	57.59	25.36	56.47	40.95	52.52	54.91	48.32
	4	13.22	62.82	22.98	60.56	36.23	57.99	51.92	51.13
	5	8.70	75.53	15.77	72.93	30.14	65.05	39.88	62.46

Adsorption isotherms

Weight loss measurements revealed that temperature and surface coverage are inversely proportional to each other. It denotes the reduced stability of the corrosion products at higher temperatures. Higher temperature may cause 1) advancement in kinetic oxidation reaction 2) increased rate of desorption. Moreover, the electrical

charge on the metal surface rises with temperature, indicating a reverse relation between surface coverage and temperature.

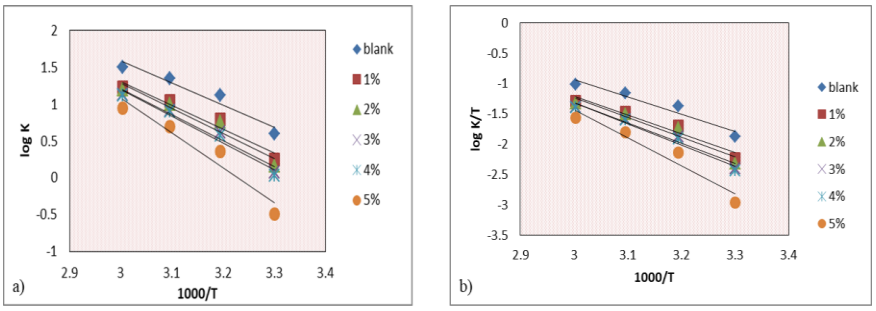

Fig. 6.4: Arrhenius plots of a) log K vs 1000/T b) log K/T vs 1000/T with and without GCE in 1 M HCl

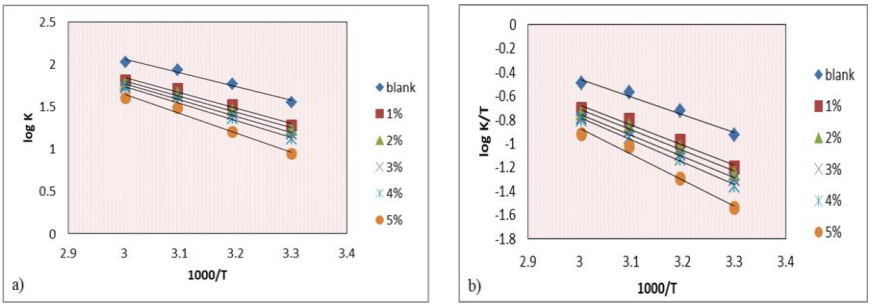

Fig. 6.5: Arrhenius plots of a) log K vs 1000/T b) log K/T vs 1000/T with and without GCE in 0.5 M H_2SO_4

Table 6.4: Thermodynamic parameters of mild steel corrosion with and without GCE in 1 M HCl and 0.5 M H_2SO_4

Medium	Conc. (v/v %)	E_a (kJ mol^{-1})	A	ΔH^* (kJ mol^{-1})	ΔS^* (J $mol^{-1}K^{-1}$)
1 M HCl	Blank	57.24	3.58×10^{10}	54.60	-44.78
	1	61.70	9.40×10^{10}	59.06	-36.76
	2	65.09	3.03×10^{11}	62.45	-27.00
	3	67.18	5.42×10^{11}	64.54	-22.19
	4	69.67	1.31×10^{12}	67.03	-14.83
	5	90.45	1.79×10^{15}	87.81	45.17
0.5 M H_2SO_4	Blank	30.96	8.16×10^{6}	28.30	-114.51
	1	34.72	1.92×10^{7}	32.08	-107.36
	2	35.72	2.54×10^{7}	33.08	-105.07
	3	36.63	3.22×10^{7}	34.01	-103.09
	4	38.32	5.50×10^{7}	35.68	-98.630
	5	43.88	3.31×10^{8}	41.24	-83.710

Adsorbed inhibitor molecules obstruct the availability of active adsorption sites on the metal surface. It may be due to the strong interaction between the inhibitor and metal surface than between the metal surface and water molecules.

Langmuir, El-Awady, Frumkin, Temkin, Freundlich and Flory-Huggins isotherms are usually employed to find the adsorption model for metal-inhibitor interaction. The best fit of all was found to be Frumkin isotherm which is a plot of log[1/c(θ/(1-θ))] vs θ for 1 M HCl. In contrast, Freundlich isotherm was found to obey in 0.5 M H_2SO_4, a plot of concentration vs θ. Fig. 6.6 a) and Fig. 6.6 b) shows Frumkin and Freundlich isotherm suited for the adsorption of GCE molecules on the metal surface in 1 M HCl and 0.5 M H_2SO_4 respectively.

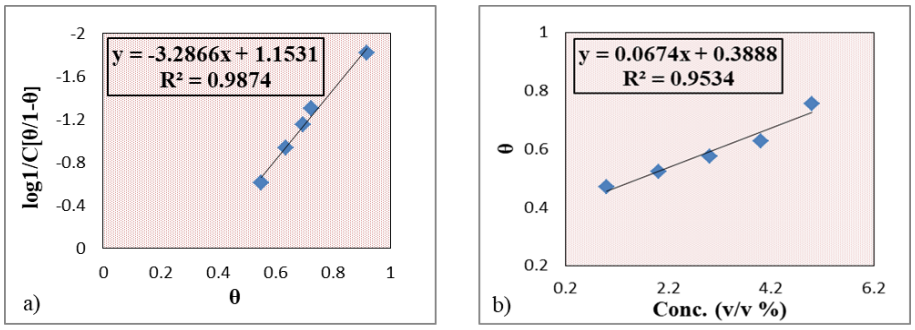

Fig. 6.6: a) Frumkin adsorption isotherm of GCE on mild steel in 1 M HCl and b) Freundlich isotherm of GCE on mild steel in 0.5 M H_2SO_4

Though the linearity of isotherm exhibited that the adsorption of GCE obeys Freundlich isotherm in H_2SO_4, appreciable deviation of the slope from unity suggested that the isotherm could not be tightly employed. The variation of the slope from unity may be described due to apparent heterogeneity on the metal surface in sulphuric acid medium[176].

From the relation between ΔG^0_{ads} and adsorption equilibrium constant K_{ads} as shown in equation (54), mechanism of adsorption of GCE molecules on the metal surface can be suggested.

$$\Delta G^0_{ads} = - RT \ln (55.5\ K_{ads}) \quad (54)$$

In the present research work, ΔG^0_{ads} for GCE-mild steel adsorptions were -26.98 and -29.70 kJ mol^{-1} in 1 M HCl and 0.5 M H_2SO_4, respectively, indicated the adsorption behaviour of GCE molecules on mild steel surface was both physisorption and chemisorption. K_{ads} values for GCE adsorption were calculated as 2572.016 and 867.227 in 1 M HCl and 0.5 M H_2SO_4, respectively. Higher value of K_{ads} pointed out that GCE molecules preferentially adsorb on the metal surface in HCl medium than H_2SO_4 medium.

UV-Visible spectroscopy

UV-Visible spectra were drawn to understand the metal-binding ability of GCE using various metal salt solutions shown in Fig. 6.7. UV spectrum of GCE displayed a maximum absorbance of 2.261 at 411 nm. Also noticed a sharp absorption band at 665 nm with an absorbance of 0.793. In addition, it showed another absorption band in the range of 505-535 nm. It can be assigned to the presence of various phytochemicals such as flavonoids, tannins, carotenoids, phenolic compounds and alkaloids. There was a sudden decrease in the intensity of these bands after binding with all the metal salts used for the present investigation. In $CoCl_2$, the maximum absorbance of 1.361 at 411 nm showed 39.9% decrease in the intensity after binding. Chromium (III) acetate revealed a maximum absorbance of 1.179 at 411 nm, implying a 47% decrease in the intensity. For Mn(II) acetate, maximum absorbance was 1.376 at 411 nm, which revealed 39% decrease in the intensity after binding. Cu(II) acetate and Zn(II) acetate exhibited a remarkable reduction in intensity as the maximum absorbance observed was 1.076 and 1.067 at 411 nm, respectively. Fe(III) chloride disclosed a maximum absorbance of 1.261 at 411 nm, with a 46% decrease in intensity. The lowering tendency was tremendous in the case of NaCl which showed 54% decrease in intensity. It may be due to quenching indicating a significant affinity of GCE towards metal salts[177].

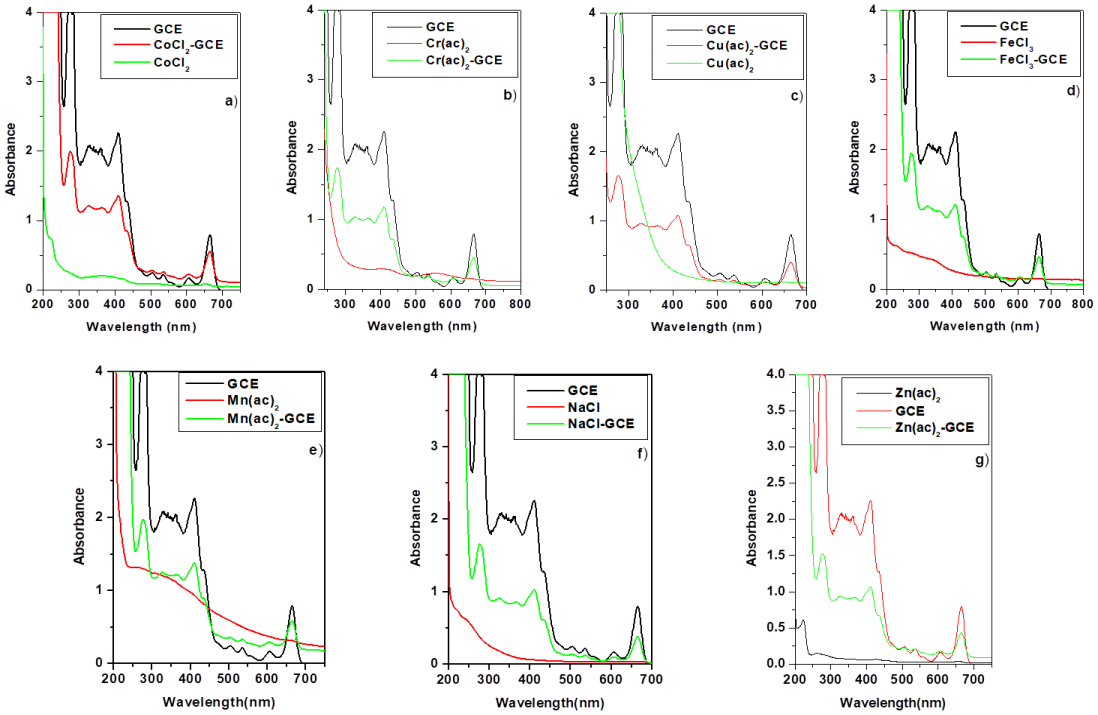

Fig. 6.7: UV spectra of a) GCE, $CoCl_2$ and GCE.$CoCl_2$ b**)** GCE, $Cr(ac)_2$ and GCE.$Cr(ac)_2$ c**)** GCE, $Cu(ac)_2$ and GCE.$Cu(ac)_2$ d**)** GCE, $FeCl_3$ and GCE.$FeCl_3$ e**)** GCE, $Mn(ac)_2$ and GCE.$Mn(ac)_2$ f**)** GCE, NaCl and GCE.NaCl g**)** GCE, $Zn(ac)_2$ and GCE.$Zn(ac)_2$

Electrochemical impedance spectroscopy

Impedance responses for mild steel corrosion in 1 M HCl and 0.5 M H_2SO_4 with and without GCE are presented in Fig. 6.8 and Fig. 6.9 as Nyquist and Bode plots, respectively. The depressed semi-circular shape of the Nyquist plot reveals that the metal dissolution process undergoes the charge transfer reaction[178]. The retarding capacity of metal corrosion by GCE molecules was realized from an increase in the diameter of the Nyquist plot with respect to concentration. Bode plots illustrate that as the concentration of GCE increased, phase angle peaks became higher and broader compared to the blank experiment. Table 6.5 outlines the result of impedance analysis assisted with Randle's equivalent circuit (Fig. 1.8). The percentage of inhibition efficiency was calculated using equation (22).

On inspection of the Table above mentioned, it was clear that R_{ct} values increased with GCE concentration, whereas C_{dl} values showed the opposite trend. The increase in R_{ct} values denotes higher inhibition efficiency by adding GCE. The drop in C_{dl} values can be ascribed to the adsorption of GCE molecules left behind water molecules at the metal solution interface. It causes the development of an adsorption layer on the mild steel surface and reduces the metal corrosion rate.

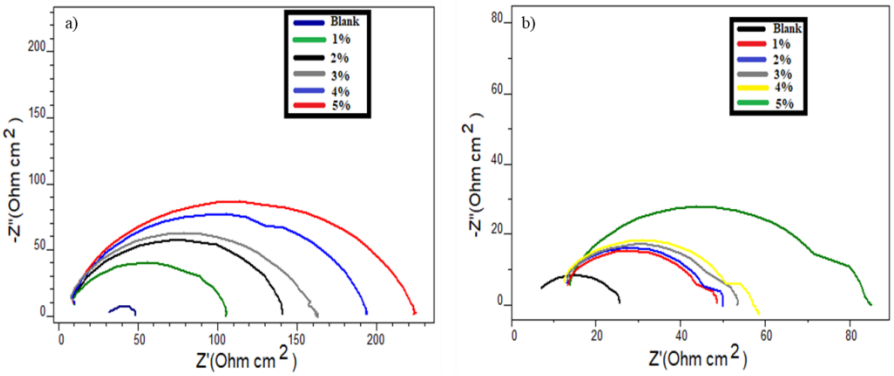

Fig. 6.8: Nyquist plots of mild steel with and without GCE in a) 1 M HCl and b) 0.5 M H_2SO_4

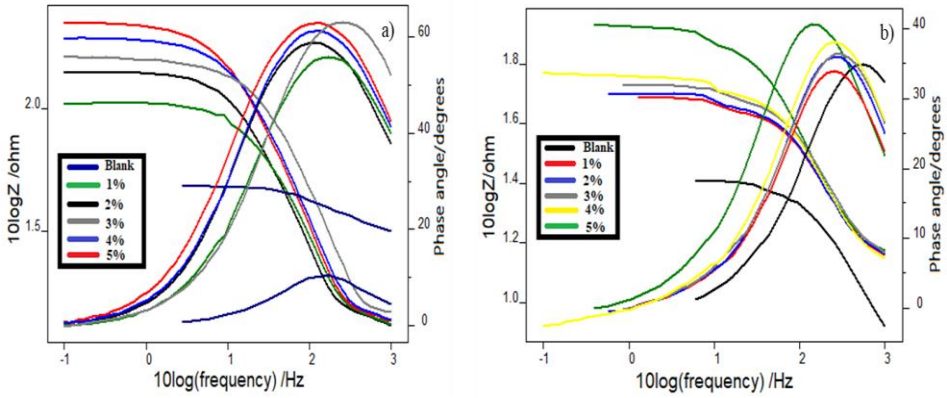

Fig. 6.9: Bode plots of mild steel with and without GCE in a) 1 M HCl and b) 0.5 M H_2SO_4

GCE showed considerably good metal protection in hydrochloric acid than sulphuric acid. In HCl, efficiency reached a maximum of 89.73%, whereas, in sulphuric acid, the extreme efficiency attained only up to 72.06%. This result was in exact agreement with weight loss measurements.

Table 6.5: Impedance parameters of mild steel in 1 M HCl and 0.5 M H_2SO_4 with and without GCE

Conc. (v/v %)	1 M HCl			0.5 M H_2SO_4		
	R_{ct} (Ωcm^2)	C_{dl} (μFcm^{-2})	η_{EIS}%	R_{ct} (Ωcm^2)	C_{dl} (μFcm^{-2})	η_{EIS}%
Blank	15.7	78.8	-	18.1	47.4	-
1	32.1	72.0	51.09	33.5	48.0	45.97
2	40.6	62.4	61.33	35.1	48.8	48.43
3	44.2	60.9	64.47	38.4	45.4	52.86
4	48.8	56.9	67.82	42.2	46.9	57.10
5	153	53.6	89.73	64.8	43.6	72.06

Potentiodynamic polarization studies

Potentiodynamic polarization studies explained changes in the anodic dissolution of mild steel and cathodic hydrogen reduction in the presence and absence of GCE as the metal corrosion controlled by redox reactions. Fig. 6.10 and Fig. 6.11 reveal Tafel and linear polarization plots in 1 M HCl and 0.5 M H_2SO_4 with varying GCE concentrations for mild steel. i_{corr} values can be obtained by extrapolating the linear fragment of the anodic and cathodic Tafel plot through the E_{corr} values. Tafel plots exhibited that GCE has appreciably changed the slope of curves at all concentrations, indicating that oxidation-reduction reactions were controlled by adding GCE into acid solutions. It may diminish the anodic dissolution of mild steel and restrict the cathodic hydrogen evolution reactions[179]. Potentiodynamic polarization parameters acquired from Tafel and linear polarization plots and corresponding calculated inhibition efficiencies are summarized in Table 6.6. From the Table, it was clear that the corrosion potential values change from negative to more positive potential moving from uninhibited metal to inhibited metal dipped in an acidic environment. But, this change was not examined in a particular direction. This fact can be considered that the reason behind GCE was acted in a mixed mode of inhibition. This trend showed that GCE molecules encourage passivation of mild steel metal as a result of interaction between GCE and the metal surface, which cause successful sealing for the surface from further reaction. The higher concentration

brings about a lower current density and attained extreme inhibition capacity of 92.51% and 74.93% in 1 M HCl and 0.5 M H_2SO_4, respectively.

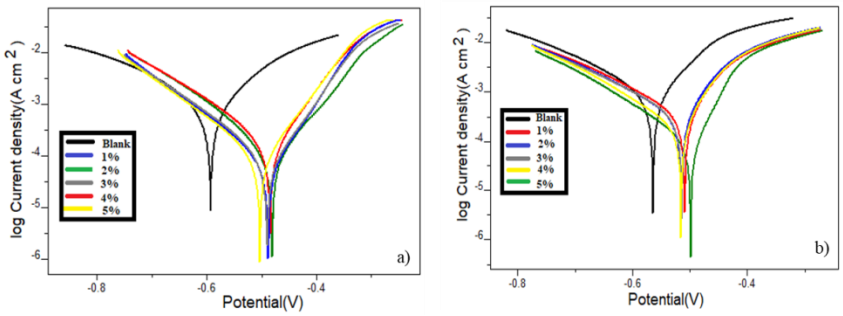

Fig. 6.10: Tafel plots of mild steel with and without GCE in a) 1 M HCl and b) 0.5 M H_2SO_4

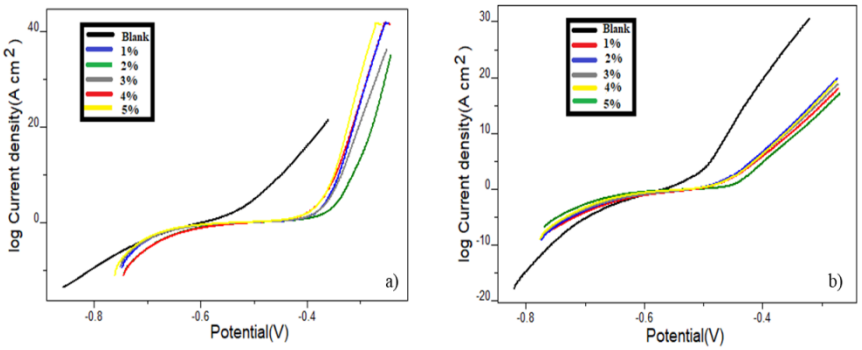

Fig. 6.11: Linear polarization plots of mild steel with and without GCE in a) 1 M HCl and b) 0.5 M H_2SO_4

Table 6.6: Potentiodynamic polarization parameters of mild steel in 1 M HCl and 0.5 M H_2SO_4 with and without GCE

Medium	Conc. (v/v %)	Tafel data					Polarization data	
		$-E_{corr}$ (mV)	i_{corr} (μAcm^2)	b_a (mV/dec)	$-b_c$ (mV/dec)	η_{pol}%	R_p (Ω)	η_{Rp}%
1 M HCl	Blank	597.9	1240	166	221	-	33.14	-
	1	492.2	441	97	172	64.43	68.92	51.91
	2	506.2	424	94	139	65.80	82.73	59.94
	3	507.3	378	104	157	69.51	84.99	61.00
	4	487.3	358	89	166	71.12	89.21	62.85
	5	495.3	92.8	72	132	92.51	217.5	84.76
0.5 M H_2SO_4	Blank	602.2	1616	184	193	-	25.30	-
	1	567.9	792	194	179	50.99	57.16	55.73
	2	574.7	743	186	174	54.02	60.06	57.87
	3	572.5	726	187	180	55.07	62.44	59.48
	4	581.6	567	176	152	64.91	82.82	69.45
	5	577.9	405	167	144	74.93	167.1	84.85

Polarization data revealed that potent corrosion inhibition could be ascribed to improved mild steel resistance against polarization when immersed in acid solutions with

GCE. In 1 M HCl polarization resistance value was 217.5 Ωcm^2 while in 0.5 M H_2SO_4, it was 167.1 Ωcm^2 at 5 v/v% GCE concentration. Due to multi-complex compounds present in the extract collected at the metal-acid interface may prevent further polarization of the mild steel, obvious from increased polarization resistance values with GCE concentration[180].

Electrochemical noise measurements

Pitting corrosion on mild steel can be easily detected from fluctuations of electrode potential. The current noise data for mild steel exposed in 1 M HCl and 0.5 M H_2SO_4 solutions with varying GCE concentrations are shown in Fig. 6.12. It exhibits that the amplitude of current noise decreased with an increase in GCE concentration, indicating the corrosion process has been dramatically prevented. PSD plots for metal dipped in 1 M HCl and 0.5 M H_2SO_4 containing various GCE concentrations are shown in Fig. 6.13. It shows that as frequency increases, magnitudes of current noise decreased. On inspecting the figure above mentioned, it is evident that the current noise for uninhibited metal was higher than inhibited metal in both acid solutions[181]. It agreed metal corrosion inhibition property of GCE in acid media was used to investigate.

Pitting index is also called pitting resistance equivalent number (PREN). It is an indicator of metal corrosion resistance[182]. Fig. 6.14 shows pitting index curves for mild steel exposed acid solutions in the absence and presence of various GCE concentrations. On examining the figure, it was clear that as GCE concentration increases, the pitting index value augments. Pitting index value was higher for the highest concentration under-study in the HCl medium, while lower in the H_2SO_4 medium for the same concentration. On comparing the pitting index values for blank and inhibited metal, it can be suggested that metal with GCE has excellent resistance power against corrosion in

the aggressive media. It also established the good anti-corrosion behaviour of GCE in 1 M HCl than 0.5 M H_2SO_4.

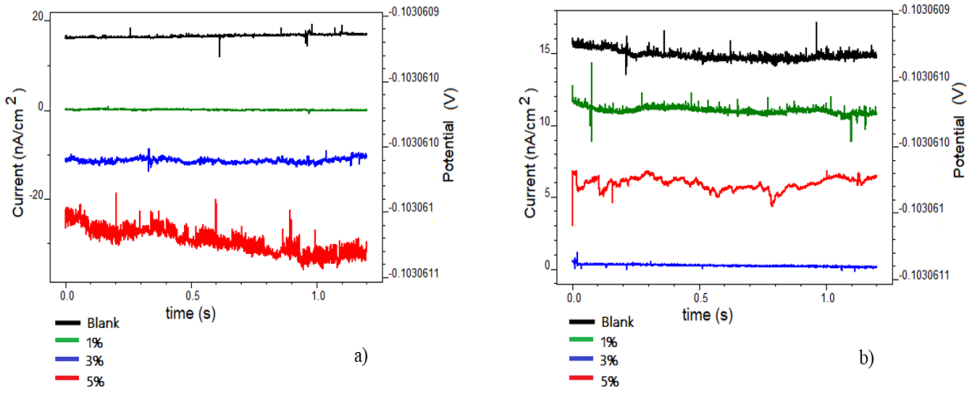

Fig. 6.12: Current noise plots of mild steel with and without GCE in a) 1 M HCl b) 0.5 M H_2SO_4

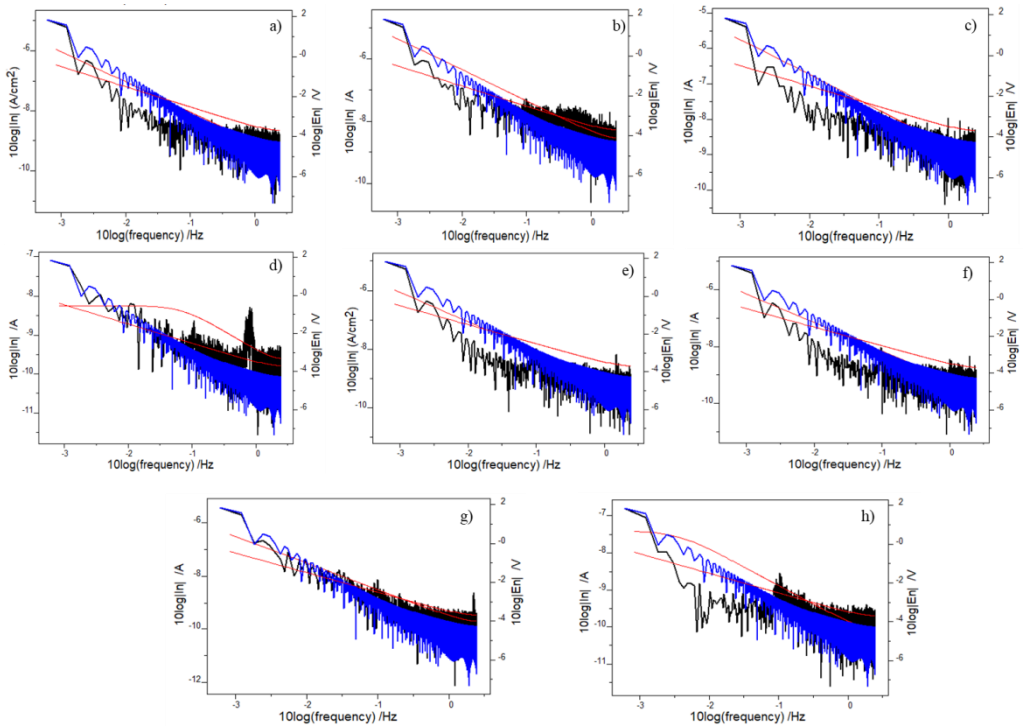

Fig. 6.13: Power spectral density plots of mild steel in 1 M HCl a) without GCE b) 1% GCE c) 3% GCE d) 5% GCE; Power spectral density plots of mild steel in 0.5 M H_2SO_4 e) without GCE f) 1% GCE g) 3% GCE h) 5% GCE

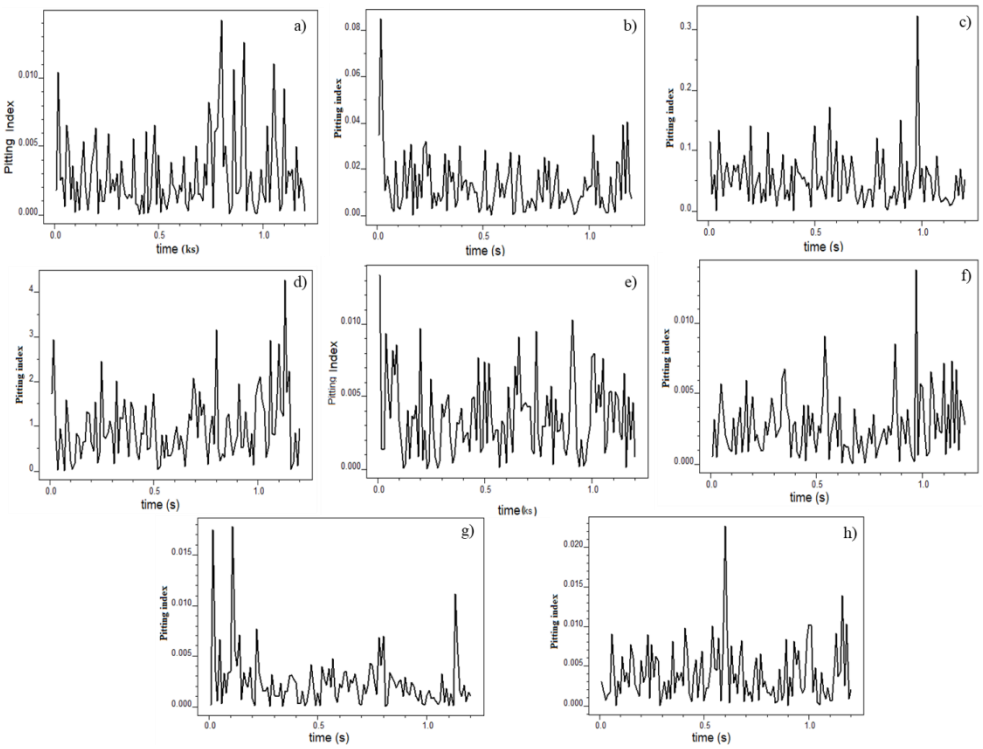

Fig. 6.14: Pitting index curves of mild steel in 1 M HCl a) without GCE b) 1% GCE c) 3% GCE d) 5% GCE; Pitting index curves of mild steel in 0.5 M H_2SO_4 e) without GCE f) 1% GCE g) 3% GCE h) 5% GCE

Atomic force microscopy

AFM analysis reinforces the surface interaction of GCE on mild steel since it is an effective method for surface morphological studies. 3-D images of AFM analysis for 24 hrs are shown in Fig. 6.15a-e. Surface roughness parameters are given in Table 6.7. Fig. 6.15 a) exhibits the surface topography of smoothened metal surface with an average roughness value (R_a) of 26.11 nm lower than the metal dipped in acid media. Fig. 6.15 b) and d) represent the corroded metal surface exposed in 1 M HCl and 0.5 M H_2SO_4, respectively. R_a values for the blank experiment were found to be higher than the metal dipped in acid solutions containing 5 v/v% GCE. Fig. 6.15 c) and e) displays the inhibited metal surfaces in 1 M HCl and 0.5 M H_2SO_4, respectively. The R_a values obtained for inhibited metal were in between smoothened metal and blank experiment. This indicates that a protective adsorption film of GCE molecules was developed on mild steel that maintained the metal surface fine and smooth. It has also been observed that

the roughness parameters for the metal with GCE in 1 M HCl were lower than in 0.5 M H_2SO_4. This fact further supported the higher inhibition power of GCE in HCl than in the H_2SO_4 medium.

Table 6.7: Surface roughness parameters of mild steel by AFM analysis

Sample	R_{pp}	R_q (nm)	R_a (nm)
Smoothened mild steel	205.27	32.92	26.11
Mild steel in 1 M HCl	965.86	79.50	55.07
Mild steel in 1 M HCl with 5 v/v% GCE	727.45	58.27	36.46
Mild steel in 0.5 M H_2SO_4	2176.62	231.72	180.48
Mild steel in 0.5 M H_2SO_4 with 5 v/v%	1026.18	120.38	86.46

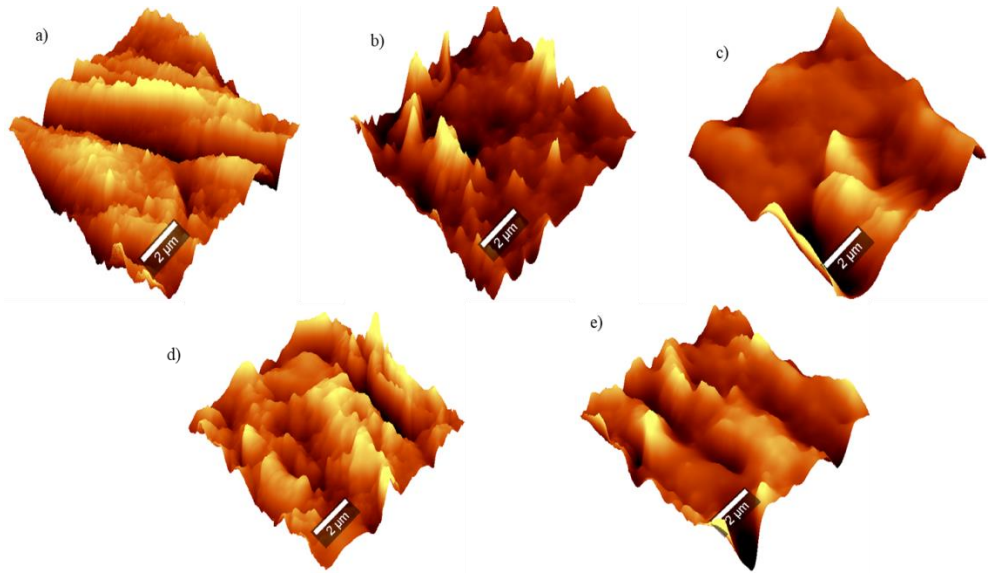

Fig. 6.15: Topography of mild steel surface a) smoothened b) in 1 M HCl c) in 1 M HCl with 5 v/v% GCE d) in 0.5 M H_2SO_4 e) in 0.5 M H_2SO_4 with 5 v/v% GCE

Quantum mechanical calculations

Spatial and electronic molecular structures of an inhibitor have a significant role in determining the inhibition potential. The optimized geometry, HOMO and LUMO of HCA and HCA lactone, two important GCE components, are shown in Fig. 6.16. Quantum mechanical parameters such as energies of HOMO (E_{HOMO}), LUMO (E_{LUMO}),

change in energy between HOMO and LUMO (ΔE), Ionisation energy (I), electron affinity (A), chemical potential (μ), electronegativity (χ), hardness (η) and the number of electrons transferred (ΔN) of HCA and HCA lactone are calculated and given in Table 6.8.

Table 6.8: Quantum mechanical parameters (in eV) of HCA (I) and HCA lactone (II)

Molecule	E_{HOMO}	E_{LUMO}	ΔE	I	A	μ	χ	η	ΔN
I	-2.131	0.090	2.22	2.13	-0.09	-1.02	1.02	1.11	2.692
II	-2.148	0.066	2.21	2.14	-0.06	-1.04	1.04	1.10	2.691

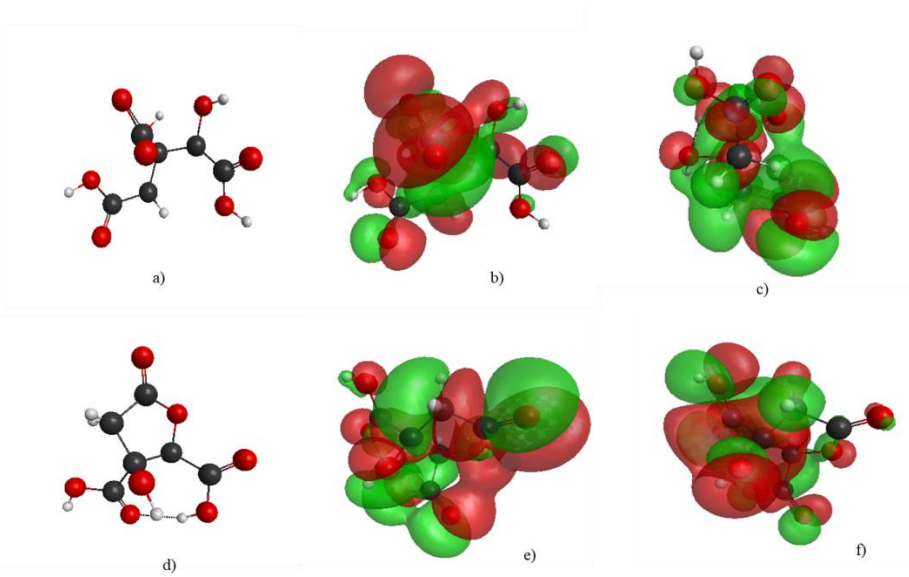

Fig. 6.16: a) Optimized geometry, b) HOMO and c) LUMO of HCA; d) Optimized geometry, e) HOMO and f) LUMO of HCA lactone

The lower change in energy (ΔE) values facilitate improved inhibition potentials as the lower ionization energy values. Table 6.8 revealed that the ΔE value for HCA lactone is smaller than HCA, indicating HCA lactone predominantly operates to decrease the energy gap and increase the possibility of electron donation. HCA also supplemented the high inhibition efficiency of GCE. The electronic chemical potential (μ) is a measure of electron's distribution in a molecule. Even though the electronic chemical potential (μ) can't predict the direction of a corrosion inhibition process, it is usually said that the adsorption of an inhibitor is encouraged by large values of μ[183]. The higher value of μ for

HCA and HCA lactone forms implies that the inhibition efficacy of GCE can be attributed to the effective interaction of these two major components.

Statistical analysis

❖ ***Optimization of factors for inhibition efficiency (IE%)***

Weight loss measurements showed that temperature, GCE concentration, and acid concentration considerably affected corrosion inhibition potential. So they opted as independent factors in this investigation. The Box-Behnken Design (BBD) structure and the three levels depending on the design of test factors (X_1, X_2 & X_3) for HCl and H_2SO_4 are shown in Table 6.9 and Table 6.10, respectively, incorporating experimental results and predicted response. A total of 15 experimental runs were found in it. It was described that corrosion inhibition efficiency is directly proportional to GCE concentration. This method attained an extreme inhibition efficiency with 5 v/v% GCE concentration in 0.5 M HCl and H_2SO_4 at 313 K. By applying RSM for the optimization, excellent efficiency was derived for the proper combination of the three factors used in the present analysis. The regression model was generated for the relation between test factors (X_1, X_2 & X_3) and inhibition efficiency, and they are shown in the quadratic equation (55) and (56) for HCl and H_2SO_4, respectively.

$$IE = 670 – 3.32\ X_1 + 27.55X_2 – 99.7\ X_3 + 0.00436\ X_1^2 + 0.013\ X_2^2 - 2.09\ X_3^2 - 0.0673\ X_1X_2 + 0.2833\ X_1X_3 + 0.841\ X_2X_3 \quad (55)$$

$$IE = 461 – 2.12\ X_1 + 4.44X_2 – 90.4\ X_3 + 0.00255\ X_1^2 + 0.349\ X_2^2 + 3.29\ X_3^2 - 0.0028\ X_1X_2 + 0.2337\ X_1X_3 + 0.287\ X_2X_3 \quad (56)$$

where IE represents inhibition efficiency, X_1 denotes temperature, X_2 denotes GCE concentration and X_3 denotes acid concentration.

Analysis of variance (ANOVA) was developed by applying this regression model[184]. ANOVA results with a significance level of 95% for HCl and H_2SO_4 are given

in Table 6.11 and Table 6.12, respectively. P-value is the most requiring value in this Table, which determine whether the factor is significant or not. The degree of essentialness (α) was selected to be 0.05. On close observation of the Table, it displayed that P-value was lower than 0.05 for linear and two-way interaction terms in HCl, whereas the linear and square term of GCE concentration has a P-value lower than 0.05. It explained that temperature, GCE concentration and acid concentration are the more significant terms. Pareto charts (Fig. 6.17) interpret that linear term GCE concentration has the most remarkable impact on inhibition efficiency in both acid media.

The better fit model for experimental data can be predicted by the closeness of R^2 and R^2(adj) value to unity. R^2 and R^2(adj) values obtained 0.9983 and 0.9954 for HCl and 0.9962 and 0.9895 for H_2SO_4, respectively. These values clearly proposed the best fit predicted model for experimental data. Therefore, the results can be quickly evaluated by the model.

Table 6.9: Experimental and predicted IE% from weight loss measurements and BBD in HCl medium

Run order	Actual level of factors			IE%		Residual
	X_1	X_2	X_3	Experimental	Predicted	
1	313	1	1	52.48	53.00	2.348
2	333	1	1	47.18	47.30	0.886
3	313	5	1	82.76	82.64	0.886
4	333	5	1	72.08	71.56	2.348
5	313	3	0.5	74.27	73.59	0.282
6	333	3	0.5	62.66	62.37	2.952
7	313	3	1.5	60.61	60.90	2.952
8	333	3	1.5	54.66	55.35	0.282
9	323	1	0.5	54.79	54.96	2.066
10	323	5	0.5	79.43	80.23	0.603
11	323	1	1.5	44.22	43.42	0.603
12	323	5	1.5	72.22	72.05	2.066
13	323	3	1	63.14	63.14	0.001
14	323	3	1	63.14	63.14	0.001
15	323	3	1	63.14	63.14	0.001

Table 6.10: Experimental and predicted IE% from weight loss measurements and BBD in H_2SO_4 medium

Run order	Actual level of factors			IE%		Residual
	X_1	X_2	X_3	Experimental	Predicted	
1	313	1	1	39.60	39.53	0.062
2	333	1	1	35.82	34.80	1.028
3	313	5	1	62.23	63.26	-1.028
4	333	5	1	58.23	58.29	-0.062
5	313	3	0.5	56.47	55.71	0.758
6	333	3	0.5	48.32	48.53	-0.207
7	313	3	1.5	46.13	45.92	0.207
8	333	3	1.5	42.65	43.41	-0.758
9	323	1	0.5	40.92	41.74	-0.821
10	323	5	0.5	65.05	64.78	0.269
11	323	1	1.5	33.45	33.72	-0.269
12	323	5	1.5	58.72	57.90	0.821
13	323	3	1	47.32	47.32	0
14	323	3	1	47.32	47.32	0
15	323	3	1	47.32	47.32	0

Table 6.11: Analysis of variance for IE% in HCl medium

Source	DF	Adj SS	Adj MS	F-Value	P-Value
Model	9	1807.96	200.88	335.49	0.000
Linear	3	1788.01	596.00	995.35	0.000
Temperature	1	140.67	140.67	234.92	0.000
GCE Conc.	1	1452.89	1452.89	2426.37	0.000
Acid Conc.	1	194.46	194.46	324.76	0.000
Square	3	1.86	0.62	1.04	0.452
Temperature*Temperature	1	0.70	0.70	1.17	0.328
GCE Conc.*GCE Conc.	1	0.01	0.01	0.02	0.906
Acid Conc.*Acid Conc.	1	1.01	1.01	1.68	0.251
2-Way Interaction	3	18.09	6.03	10.07	0.015
Temperature*GCE Conc.	1	7.24	7.24	12.09	0.018
Temperature*Acid Conc.	1	8.02	8.02	13.40	0.015
GCE Conc.*Acid Conc.	1	2.83	2.83	4.72	0.082
Error	5	2.99	0.60		
Lack-of-Fit	3	2.99	1.00	*	*
Pure Error	2	0.00	0.00		
Total	14	1810.96			

DF: degrees of freedom, Adj SS: adjusted sum of squares, Adj MS: adjusted mean of squares, F: Fischer's F-test value, P: probability

Table 6.12: Analysis of variance for IE% in H_2SO_4 medium

Source	DF	Adj SS	Adj MS	F-Value	P-Value
Model	9	1287.93	143.10	147.40	0.000
Linear	3	1273.00	424.33	437.08	0.000
Temperature	1	47.06	47.06	48.47	0.001
GCE Conc.	1	1114.86	1114.86	1148.34	0.000
Acid Conc.	1	111.08	111.08	114.42	0.000
Square	3	9.13	3.04	3.13	0.125
Temperature*Temperature	1	0.24	0.24	0.25	0.640
GCE Conc.*GCE Conc.	1	7.20	7.20	7.41	0.042
Acid Conc.*Acid Conc.	1	2.49	2.49	2.57	0.170
2-Way Interaction	3	5.80	1.93	1.99	0.234
Temperature*GCE Conc.	1	0.01	0.01	0.01	0.913
Temperature*Acid Conc.	1	5.46	5.46	5.63	0.064
GCE Conc.*Acid Conc.	1	0.33	0.33	0.34	0.586
Error	5	4.85	0.97		
Lack-of-Fit	3	4.85	1.62	*	*
Pure Error	2	0.00	0.00		
Total	14	1292.78			

DF: degrees of freedom, Adj SS: adjusted sum of squares, Adj MS: adjusted mean of squares, F: Fischer's F-test value, P: probability

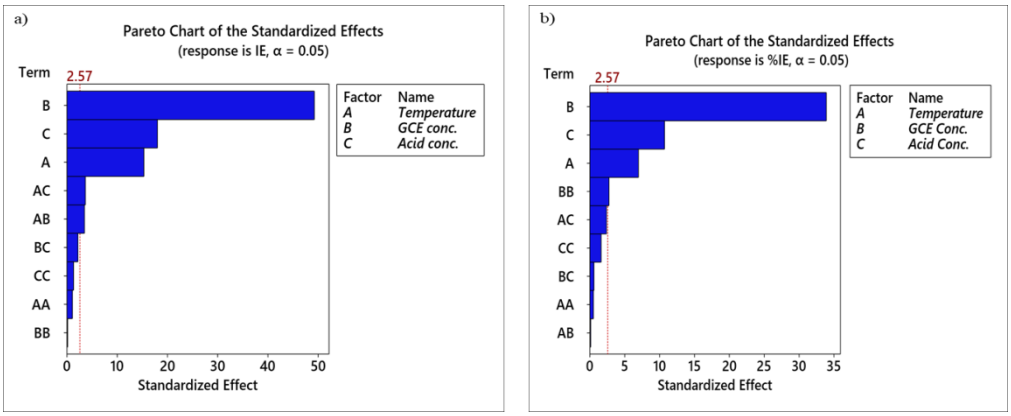

Fig. 6.17: Pareto chart of the standardized effects of mild steel in a) HCl b) H_2SO_4 medium

Main effects plots complement the results from the regression analysis. It illustrates the influence of tested factors on response. Fig. 6.18 shows the main effects plots for the fitted means of inhibition efficiency in HCl and H_2SO_4 media. On analyzing the figure above mentioned, it has been noticed that the maximum inhibition efficiency was with 5 v/v% concentration of GCE at an operating temperature of 313 K at 0.5 M concentration of HCl and H_2SO_4. As temperature rises, the kinetic energy of the inhibitor

molecules enhances and thereby, the velocity of bombardment between the molecules increases. This inclination tends to break down the formation of adsorbed film by inhibitors on the metal surface and decreases inhibition efficiency. A similar observation was found with an increase in acid concentration. At the same time, the inhibition capacity of GCE gets boosted by the addition of 1 to 5 v/v% GCE concentration. In the presence of inhibitor, the corrosion rate was decreased due to the adsorption of inhibitor molecules, and efficiency also increases.

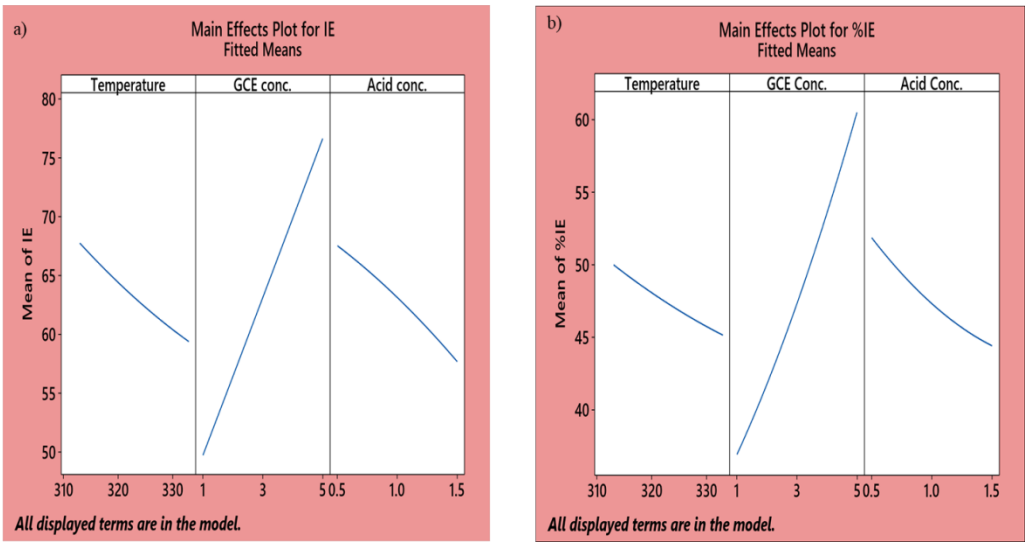

Fig. 6.18: Main effects plots for inhibition efficiency of mild steel in a) HCl b) H_2SO_4 medium

Fig. 6.19 reveals the interaction plot for inhibition efficiency in two acids which interprets any interaction between factors. If there are any crossed lines in the interaction plot, it will designate a significant interaction between the factors. Parallel or straight lines imply that there is no interaction between factors. From Fig. 6.19, it has been observed that the two-way interaction terms were inessential as there are no crossed lines in the interaction plot for inhibition efficiency in both acids. However, in HCl and H_2SO_4, parallel lines between temperature and acid concentration were not perfect, indicating some interaction. ANOVA analysis was also supplemented with these results.

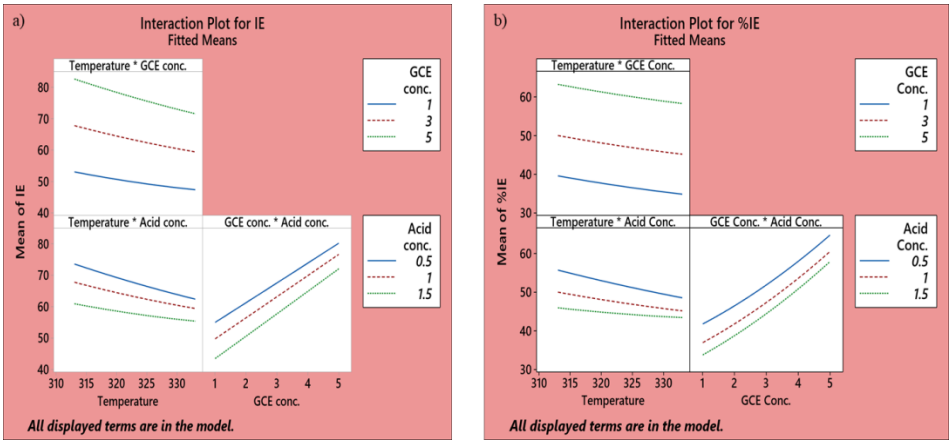

Fig. 6.19: Interaction plot for inhibition efficiency in a) HCl b) H_2SO_4 medium

Contours and 3-D surface plots delineate the inter-dependence of the tested factors on IE% and are shown in Fig. 6.20 and Fig. 6.21. It displayed that the inhibition efficiency grows tremendously when GCE concentration increases at a particular temperature. Whereas inhibition efficiency drop-down when the temperature rises. This IE%-temperature relationship can be attributed to the physical adsorption of GCE molecules on the mild steel surface. Inhibition efficiency and acid concentration are inversely proportional, indicating a higher concentration of aggressive media corrodes metal dramatically.

❖ ***Response optimization***

Quadratic equations (55) and (56) were used to optimize the independent factors such as temperature, GCE concentration and acid concentration to maximize IE. For the outstanding response, the desirability function method was adopted. Response optimization plots for IE in both media are shown in Fig. 6.22. The anticipated optimum factors observed were temperature of 313 K, GCE concentration of 5 v/v%, and acid concentration of 0.5 M and the corresponding predicted IE were 87.62% and 68.69% in HCl and H_2SO_4 solutions, respectively. Confirmation tests have been attained the perfect optimal factor settings and betterment of IE.

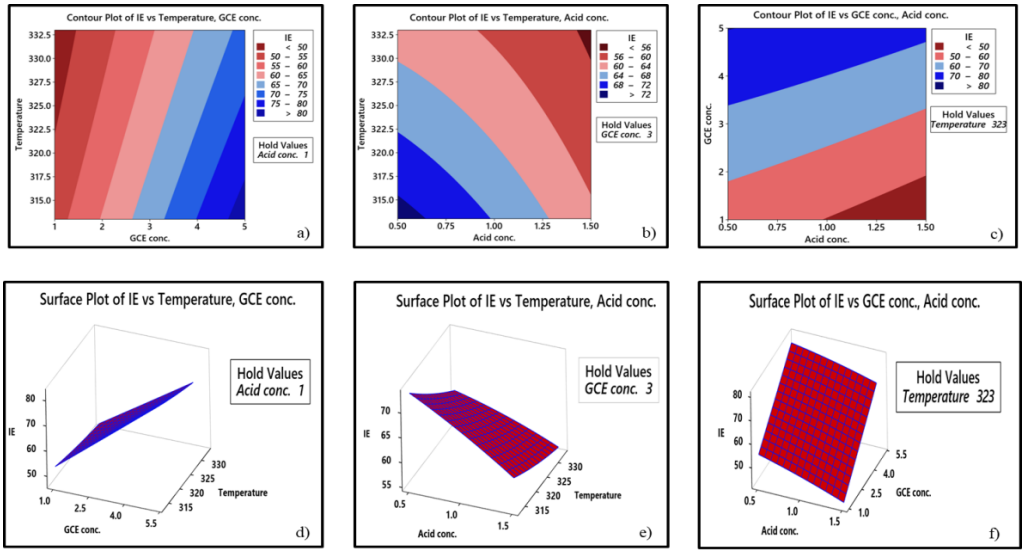

Fig. 6.20: a, b & c) Contours and d, e & f) 3-D surface plots for inhibition efficiency in HCl

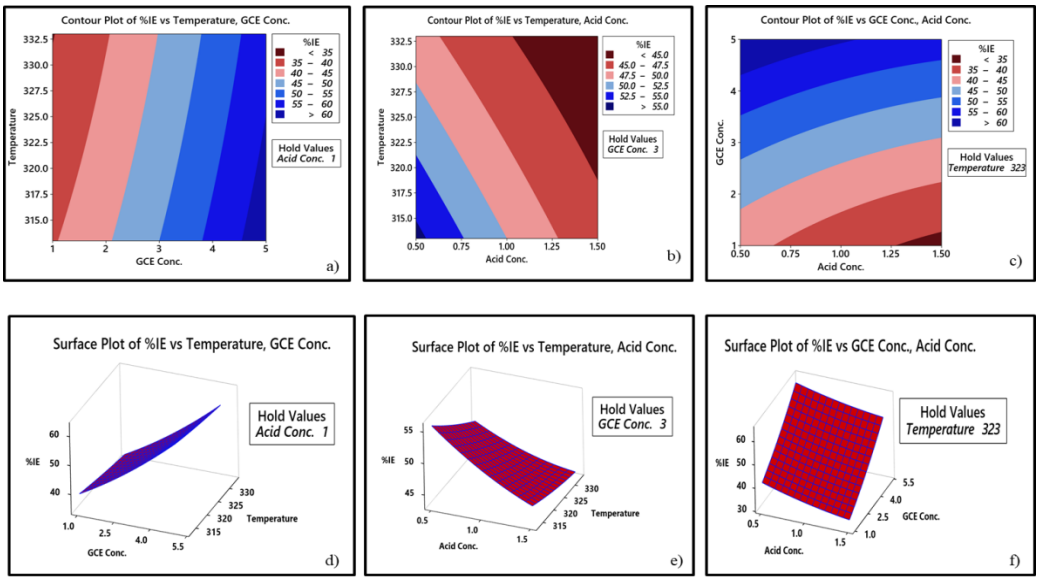

Fig. 6.21: a, b & c) Contours and d, e & f) 3-D surface plots for inhibition efficiency in H_2SO_4

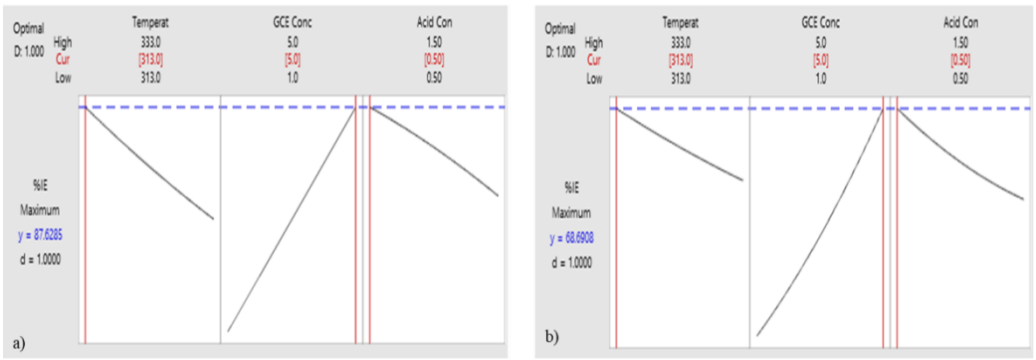

Fig. 6.22: Response optimization plot for inhibition efficiency in a) HCl b) H_2SO_4 medium

Conclusions

- *Garcinia cambogia* extract (GCE) acts as an efficient green inhibitor for corrosion of mild steel in 1 M HCl and 0.5 M H_2SO_4 medium. As the concentration of the inhibitor increases, the protecting power also increases.
- On comparing, GCE in 1 M HCl medium shows higher efficiency than 0.5 M H_2SO_4 medium. GCE exhibited 91.73% at 5 v/v% inhibition efficiency in 1 M HCL medium whereas it showed 75.53% at 5 v/v% in 0.5 M H_2SO_4 medium.
- UV-Visible spectra of extract solutions suggests the binding ability of GCE with various metals.
- Temperature and inhibition efficiency is in inverse proportional relation.
- Electrochemical impedance analysis exhibits that charge transfer resistance increases and double layer capacitance decreases according to GCE concentration.
- Potentiodynamic polarization measurements exhibit mixed type character of inhibition for GCE.
- Sharp decrease in corrosion current density pointed out that there is strong resistance in the corrosion process.
- Quantum mechanical calculations of major components - hydroxycitric acid (HCA) and hydroxycitric acid lactone (HCA lactone) present in GCE support the inhibition power of GCE.
- The adsorption studies of GCE shows that it obeys Langmuir adsorption isotherm.
- Atomic force microscopy of metal surfaces exposed in acid media with and without GCE also confirmed the protecting power of GCE.

- Statistical analysis also verified the effect of temperature and concentration of GCE and concentration of acid (both HCl and H_2SO_4) on inhibition efficiency.